Journal of Applied Polymer Science

Development of Elastic and Plastic Properties of Polyoxymethylene During Bending Fatigue

Gregory S. Heinlein, Shannon J. Timpe
Department of Mechanical Engineering, Bradley University, Peoria, Illinois 61625
Correspondence to: S. J. Timpe (E-mail: sjtimpe@bradley.edu)

ABSTRACT: The development of the plastic and viscoelastic properties and the corresponding failure limits of the acetal homopolymer polyoxymethylene were studied in unidirectional cyclic fatigue. Samples with molecular weights (MWs) ranging from 90 to 142 kg/kmol were tested in displacement-controlled conditions, resulting in maximum stress amplitudes between 30 and 59 MPa and strain amplitudes between 35.8 and 92.6 $\mu\varepsilon$. The zero-hour material properties and the cycle-dependent property development were predominantly dictated by deformations in the crystalline regions and showed a negligible dependence on MW. However, the final failure limits were found to be primarily dependent on the length of the amorphous tie chains that connect the crystallites. As such, fatigue life analysis showed a strong dependence on MW. Results are interpreted in light of the primary mechanical failure mechanisms and the corresponding molecular deformations. © 2014 Wiley Periodicals, Inc. J. Appl. Polym. Sci. **2014**, *131*, 40762.

KEYWORDS: mechanical properties; properties and characterization; thermal properties; thermoplastics; viscosity and viscoelasticity

Received 10 November 2013; accepted 24 March 2014
DOI: 10.1002/app.40762

INTRODUCTION

Polyoxymethylene (POM), a polyacetal resin, is a common engineering thermoplastic with excellent toughness, moldability, and dimensional stability.[1–3] Because of the advantageous properties, POM is used extensively in applications ranging from conventional injection-molded or extruded components to microscale devices.[4–7] Expanding applications have resulted in engineering requirements for greater plastic and viscoelastic property stability over longer product lifetimes. Accordingly, a more complete understanding of the development of mechanical and dynamic properties and degradative phenomena is essential.

As polyacetal polymers solidify during the injection molding process, the material forms a semicrystalline structure of roughly circular spherulites. These structures are composed of radially arranged lamellae connected by chain-entangled amorphous regions. Various researchers have linked polymer mechanical behavior under various macroscale deformation conditions to the mechanisms of molecular motion.[6–11] Under low strain, the main mechanism is the movement of the lamellae relative to one another, known as interlamellar sliding. As the strain is increased, the lamellae begin to separate. However, the macrostructure is still held together via amorphous region tie chains that connect the crystalline lamellae. In this deformation regime, strain behavior is dictated by the number, length, and entanglement of the tie chains. Plummer et al.[12] found that, with a high supercooling rate such as that commonly found in injection molding, amorphous region entanglement does not vary significantly with molecular weight (MW). Therefore, although the relationship between stress and strain (associated with entanglement) is not expected to show significant MW dependence, the final strain limits (associated with chain length) may be influenced by MW.

The reorganization and deformation of the crystalline structure due to molecular motion of the polymer chains during cyclic loading results in mechanical property changes.[13–18] Stress- and strain-controlled cyclic loading of acetal specimens have been found to display softening behavior at high stress levels and loading frequencies.[13–18] It has been experimentally shown that stress softening is related to a temperature rise in the sample and that stress hardening is related to lamellae reorganization.[14]

Rheological properties of polymers have been phenomenologically described using a variety of theoretical models.[19–21] These models show that chain motion and stress relaxation times show a power law dependence on MW. These models have shown good agreement with experiments in predicting the viscoelastic properties of various polymers.[22–25]

In addition to the development of mechanical properties during cyclic testing, the details of molecular chain motion also influences material failure limits. MW has been found to significantly affect fatigue life and crack propagation.[26–30] Crack

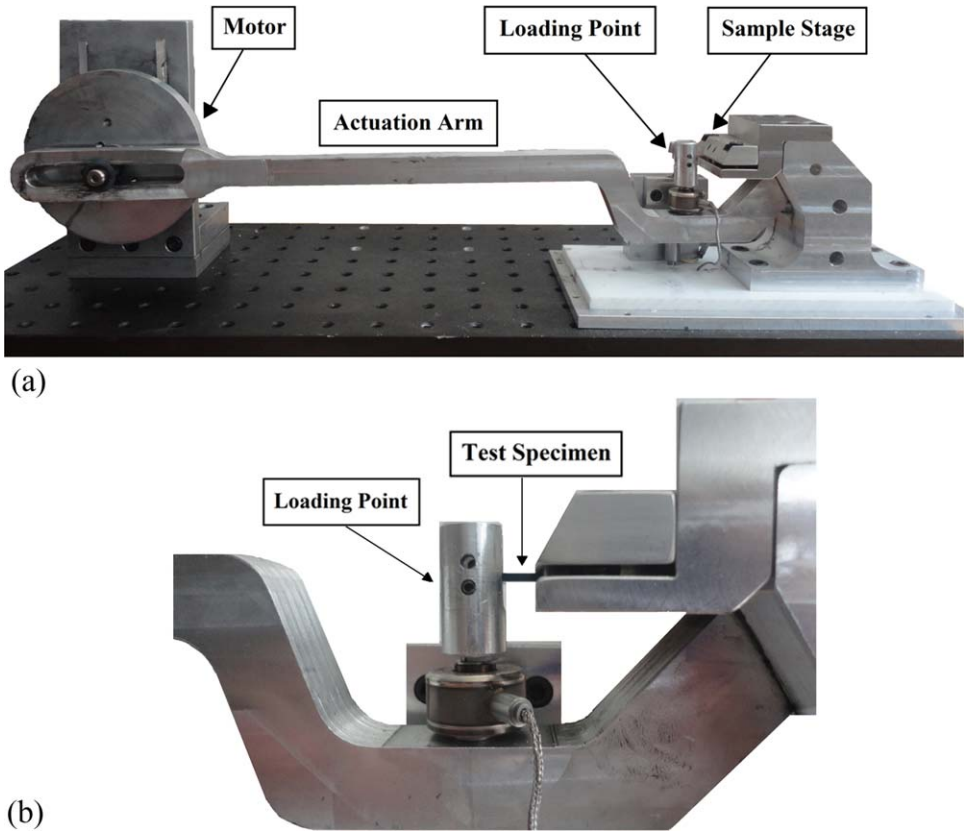

Figure 1. Images of the cyclic fatigue tester used to determine the properties of cantilevered polyoxymethylene samples showing (a) the full device and (b) a close-up view of the loading region. [Color figure can be viewed in the online issue, which is available at wileyonlinelibrary.com.]

propagation in polymers is dictated by the characteristics of the bulk crack tip as well as by the fibril bundles that bridge the gap, adding toughness. Increases in MW result in longer fibril bridges, thereby increasing the fracture toughness and fatigue failure limits.

In the current study, development of mechanical properties was monitored in cyclically loaded POM samples. The macrostructure of POM dictates the material properties. Thus, a thorough understanding of the development of plastic and viscoelastic properties can reveal the underlying polymeric deformation mechanisms. Property development results and the resultant fatigue limits are interpreted in light of the principal molecular deformation mechanisms and changes in the organization of the acetal chains.

EXPERIMENTAL

The current research used commercial un-crosslinked linear POM, $(CH_2O)_n$—Delrin® 100P, Delrin® 311DP, and Delrin® 900P (E. I. du Pont de Nemours and Company). Cantilever-style fatigue samples were fabricated using a Nissei FN4000 injection molding machine with a 40-mm screw and barrel operating with a melt temperature of 215°C, a mold temperature of 90°C, and a pack pressure of 60 MPa. The pack time for the mold was 35 sec, with a 10 sec cooling time and a 49 sec overall molding cycle. Samples were formed in a four-cavity cold runner mold with a thickness in the loading direction of 1.65 mm, a width of 4.3 mm, and a length of 10.2 mm. Samples contain a 0.30 mm fillet parallel to the width dimension to decouple the behavior from the applied clamping force.

Molecular Weight Measurements

The average MW for each class of polymer was determined using size exclusion chromatography. Filtered dilute solutions of POM in hexafluoroisopropanol were measured using a Waters Corp. Model Alliance 2695™ system. The system was equipped with viscosity, refractive index, and light scattering detectors that allowed accurate determination of MW, without reference to universal standards. Five samples of each polymer class were tested.

Thermodynamic Property Measurements

Thermodynamic properties for each polymer class were measured using a differential scanning calorimeter (TA Instruments, Q2000). Samples were heated and cooled at a rate of 10°C/min with a peak temperature of 220°C. Five samples of each polymer class were tested. Several relevant material properties were extracted from the thermodynamic testing, including the percentage crystallinity and the peak melt temperature. The peak melt temperature, i.e., the melt temperature during the first heating cycle, was also used to extract the estimated lamellar thickness, l, according to the relationship:[12]

$$l = \frac{2\sigma_e T_{\mathrm{mo}}}{\Delta h_o (T_{\mathrm{mo}} - T_m)} \quad (1)$$

where T_m is the measured melt temperature, T_{mo} is the melt temperature of the ideal crystal (=200°C)[12], Δh_o is the heat of

fusion per unit volume ($=380 \times 10^6$ J m^{-3})[12], and σ_e is the chain fold surface energy ($=0.125$ J m^{-2})[12].

Mechanical Property Measurements

The development of the elastic and plastic material properties was measured using the custom-built unilateral cyclic loading apparatus shown in Figure 1. Cyclic loading was initiated using a variable speed servomotor (Kollmorgen, AKM21C). Rotation of the servomotor led to oscillatory motion of the actuation lever arm, which, in turn, caused a known displacement at the loading point. This will be referred to as the maximum displacement magnitude for a given test. A pin provided single point loading to bend the sample. A miniature load cell (Honeywell, Model 31) is attached to the lever arm below the loading pin to record the force response during testing. A linear variable differential transformer (Ametek, Model M00060JLP02) is attached to the loading pin to record the displacement.

Samples were clamped behind the fillet to a torque of 4.25 N m and tested at a constant cyclic loading frequency of 6.67 Hz. Loading was performed in a unidirectional configuration, with samples relaxing freely during the unloading portion of the cycle. Displacement can be converted to strain using the standard Euler–Bernoulli equations for elastic bending

$$\varepsilon_{max} = \frac{3 y_{max} h}{2L^2} \quad (2)$$

where, ε_{max} is the maximum strain for a given cycle, y_{max} is the maximum displacement at the loading point, h is the thickness of the beam ($=1.65$ mm), and L is the beam length ($=10.2$ mm). Although some plastic deformation occurs during testing, the deformed sample shape does not deviate significantly from the Euler–Bernoulli estimations. Thus, utilization of the elastic calculations is deemed appropriate.[13]

As a result of the free relaxation of the sample during unloading, material creep alters the equilibrium rest position over the course of cyclic testing. Accordingly, critical calculations were performed based on the actual strain from the instantaneous equilibrium position. Because the beam is allowed to relax to a zero instantaneous strain, the strain amplitude for fatigue characterization is equal to the maximum strain.

The maximum flexural stress at the outer surface of an end loaded constant cross-section beam is given by

$$\sigma_{max} = \frac{P_{max} L h}{2I} \quad (3)$$

where P_{max} is the maximum applied load for a given cycle and I is the moment of inertia ($=1.28$ mm^4). Because the beam is allowed to relax to a zero externally applied stress, the instantaneous stress amplitude is equal to half of the observed maximum stress. However, because displacement-controlled tests were performed, the stress amplitude changes with each subsequent cycle. As such, the stress amplitudes used in the proceeding analyses represent the averages over the sample lifetimes.

Tests were performed at maximum displacement values ranging from 2.0 to 6.5 mm, corresponding to strain amplitude values between 35.8 and 92.6 $\mu\varepsilon$. These displacements provided a range of observed stress amplitudes between 30 and 59 MPa. All tests were performed at room temperature and ambient humidity conditions.

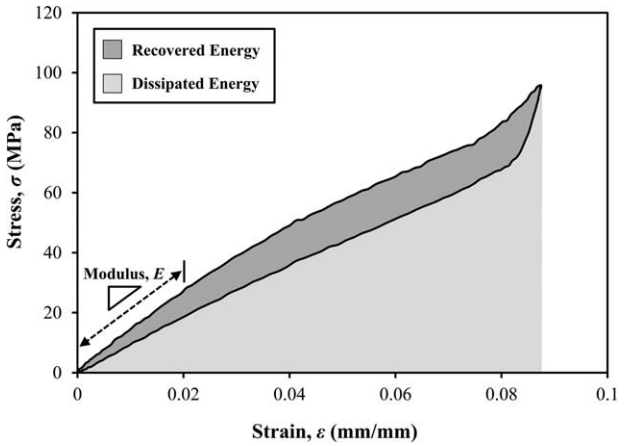

Figure 2. Characteristic stress–strain hysteresis loop displaying the principal mechanical property calculations including the elastic modulus and the dissipated and recovered energies. The sum of the dissipated and recovered energies is the total input strain energy.

To clarify the analysis methodology, a characteristic stress vs. strain cycle is shown in Figure 2. The relationship between the stress and the strain is determined by calculating the slope of the initial 2% strain of the loading portion of the hysteresis loop (i.e., the linear portion). Because this slope encapsulates the stress–strain relationship, it is termed the modulus. However, due to the plastic deformation and changing equilibrium point resulting from creep, this modulus should not be directly compared with flexure or tensile moduli reported for other deformation configurations.

The hysteresis behavior can also be analyzed to determine the relative contributions of elastic and plastic work. The energy dissipated or plastic work, W_P, is the area between the loading and unloading portions of the cycle, or the closed integral of stress vs. strain.

$$W_P = \oint \sigma d\varepsilon \quad (4)$$

This is the unrecoverable energy absorbed by the material for molecular motion and converted to heat. The recovered energy or elastic work, W_E, is the area below the hysteresis loop, or the integral of the unloading portion of the cycle.

$$W_E = \int_{unloading} \sigma d\varepsilon \quad (5)$$

The summation of these two areas is the total system energy input, W_T. Specific loss, or the ratio of the plastic work to the total work, can be used to estimate the viscoelastic phase angle, δ.

$$\frac{W_P}{W_T} = 2\pi \tan\delta \quad (6)$$

RESULTS AND DISCUSSION

Analytical Results

Size exclusion chromatography and differential scanning calorimetry tests were conducted on untested samples to examine

Table I. Analytically Measured Properties of Polyoxymethylene

Labels	Polymer	Weight-average MW (g/mol)	Crystallinity (%)[a]	Melt temperature (°C)	Lamella thickness (nm)	Molar mass dispersity (M_w/M_n)
Low MW	Delrin® 900P	91,000	56 ± 0.35	177	5.7	1.8
Medium MW	Delrin® 311DP	112,000	55 ± 0.90	178	6.0	1.9
High MW	Delrin® 100P	142,000	53 ± 0.72	178	6.0	1.8

[a] Based on a 326 J/g enthalpy for the pure crystal.

the polymeric molecular structure and the thermodynamic properties. Table I shows the key results from these tests, including MW, percentage crystallinity, melt temperature, calculated lamella thickness, and the molar mass dispersity. It can be seen that the most marked difference between the three tested materials is in the MW, with the Delrin® 100P exhibiting a relatively high average MW, Delrin® 311DP exhibiting a moderate MW, and Delrin® 900P exhibiting the lowest MW. Accordingly, to generalize the current results, the three grades of POM will be labeled by MW throughout the remainder of this document as "high" (Delrin® 100P), "medium" (Delrin® 311DP), and "low" (Delrin® 900P). The molar mass dispersity (i.e., the ratio of the weight-average MW to the number-average MW) is similar for all the three polymer types and has a value consistent with the step-polymerization process used to synthesize POM. The percentage crystallinity shows a slight decrease with increasing MW consistent with previous findings.[12] Melt temperature does not vary significantly, indicating that, although the molecular chain length varies, the crystalline lamella size is relatively stable at approximately 6 nm [see eq. (1)]. The glass-transition temperature, T_g, does not vary significantly for injection-molded POM and has a reported value near −60°C. In addition, because mechanical property testing was performed at temperatures much greater than the glass transition, any slight variations in T_g are not expected to significantly influence the current results.

By combining these analytical results with the mechanical testing described in the subsequent section, structure–property relationships can be hypothesized. Because the size and density of the lamella are similar for all the tested polymers, MW is not likely to influence mechanical properties related to crystallite deformations. However, MW will dictate properties limited by molecular chain orientation in amorphous regions, and these properties are expected to display differentiation among the polymer types.

Cyclic Testing Results

The POM samples were cyclically loaded at 6.67 Hz at various displacement levels until failure. Figure 3 shows several characteristic hysteresis loops at different intervals, based on the progression to failure (N_f) as a percentage, throughout a typical test. Although the displayed data are from a 4-mm displacement test of a low MW sample, the results can be generalized because a phenomenologically similar hysteresis loop progression was seen for all tests. Each loop is the stress vs. strain data for a single loading/unloading cycle. Several observations can be made from examining Figure 3. First, a result of the displacement control of the test is that all cycles reach approximately the same maximum strain (0.09 mm/mm in the current example). Although the historical strain is equal for all cycles, the actual strain steadily decreases as a result of permanent deformation of the sample. Because the samples are loaded unidirectionally and allowed to freely relax during unloading, the cantilever will come out of contact with the loading pin at a higher historical strain with each progressive cycle. In the current analysis, a sample is said to be out of contact when the force decreases below a certain threshold, set at 3% of the peak stress. Because of the permanent deformation, coupled with the fact that the sample is allowed to freely relax, the actual strain has been defined relative to the instantaneous zero strain rather than to the historical zero strain. Another observation regarding Figure 3 is that the maximum stress decreases with progressing cycles. This results from the lower actual input strain with each progressive cycle. Permanent sample deformation reduces the load-bearing capacity for a given deformation referenced from the original equilibrium position.

Modulus Analysis. The linear portion of the loading cycle (i.e., the modulus defined according to Figure 2) was monitored as a function of loading cycles. For each of the three polymers, the modulus is shown in Figure 4 on a log-linear scale as a function of the number of loading cycles. For clarity, only a selection of

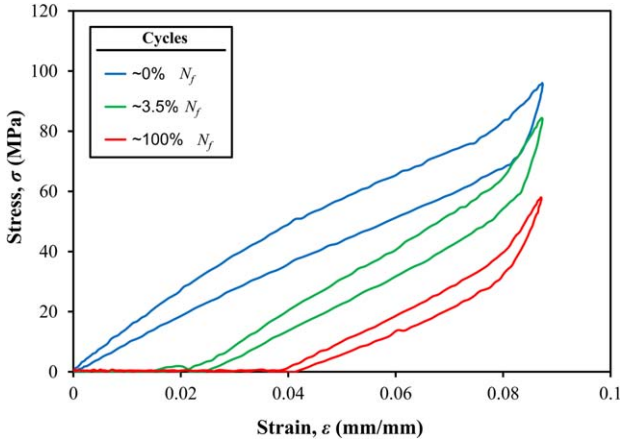

Figure 3. A characteristic data set depicting the progression of the hysteresis behavior during cyclic testing. Data are shown as a percentage of cycles to failure (N_f) corresponding to early, moderate, and late stages of progression toward failure. [Color figure can be viewed in the online issue, which is available at wileyonlinelibrary.com.]

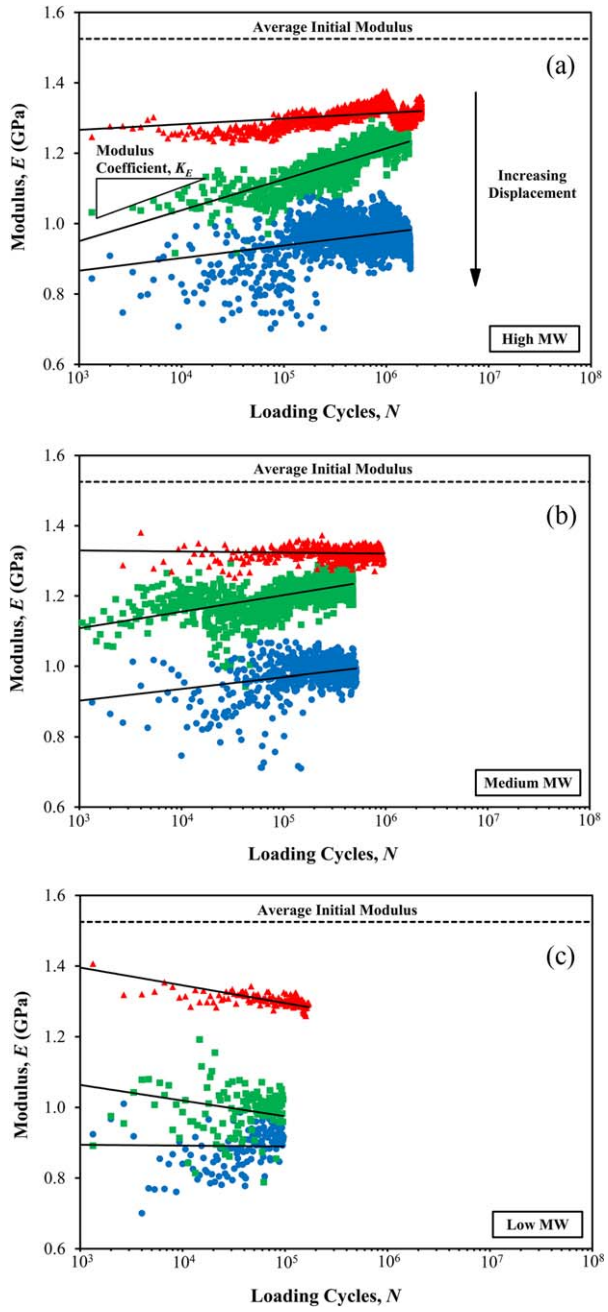

Figure 4. Characteristic data for the elastic modulus as a function of the number of bending fatigue cycles for (a) high, (b) medium, and (c) low molecular weight samples. Data is shown for each polymer type at maximum displacement magnitudes of (○) 6 mm, (□) 5 mm, and (Δ) 3 mm. [Color figure can be viewed in the online issue, which is available at wileyonlinelibrary.com.]

the modulus development data sets are shown. Each sub-figure displays three different tests, corresponding to three different maximum displacements. Logarithmic trend lines are shown to characterize the development of the modulus.

The modulus was observed to decrease rapidly in the first few cycles. The average initial modulus (measured on the first loading cycle) is shown as a dashed line in Figure 4. The initial modulus decrease can be observed by comparing this initial modulus with the Figure 4 data points. Within the first few stress cycles, molecular deformation leads to a stress softening effect and a general decrease in the modulus. In order to quantify the rapid change, Figure 5 shows the average modulus between 10^4 and 10^5 cycles as a function of the measured stress amplitude. As stress amplitude increases, a larger initial decrease is observed. With increased deformation, additional dissipated plastic energy is directly converted to heat. This provides the thermal energy necessary for enhanced molecular motion and leads to an overall decrease in stiffness. These results are consistent with previous research attributing stress softening to hysteretic heating in cyclically loaded polymers.[14–17] In addition, it can be seen that the initial decrease in the modulus has a negligible dependence on MW. Therefore, the molecular motions are dominated by crystallite deformations. As seen in Table I, lamella size, and therefore crystallite deformation, is MW independent.

After the rapid, initial decrease in the modulus, a log-linear change occurs with respect to cycles as seen in Figure 4. Although the log-linear trend was observed for all tests, higher displacement test conditions lead to an increased data scatter. This is attributed to variation in crystallinity and lamella size throughout the material, leading to highly variable mechanical behavior,[31,32] which is exacerbated by an increased contribution of local damage at higher loads. In order to quantify changes in the modulus during this portion of the test, logarithmic trend lines were developed for the data in Figure 4. The slope of the logarithmic curve fit will be termed the modulus coefficient, K_E, having units of GPa per ln(cycles). Figure 6 shows the modulus coefficient as a function of the MW. Each data point represents a single test, and the overlaid box plots show the sample median, the first and third quartiles, and whiskers at ±1.5 times the interquartile range. The high, medium, and low MW samples show modulus coefficient mean values of 0.023, 0.015, and −0.010, respectively. An analysis of variance test concluded that the high and medium MW samples were statistically different, with a confidence interval of 90%. However, each showed a marked difference from the low MW samples with a statistical

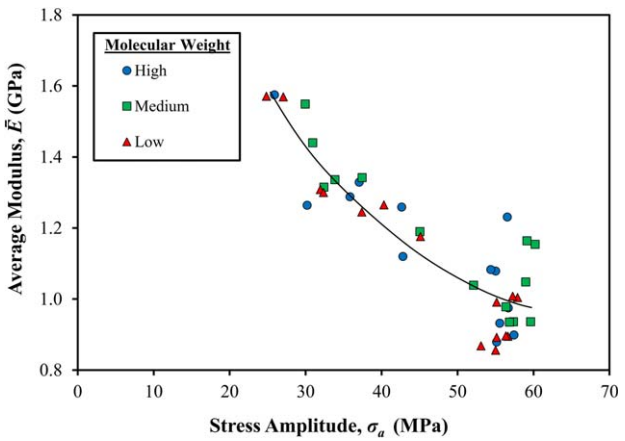

Figure 5. Average modulus between 10^4 and 10^5 cycles as a function of the stress amplitude. Each data point represents a measurement of a single sample tested at a single displacement level. [Color figure can be viewed in the online issue, which is available at wileyonlinelibrary.com.]

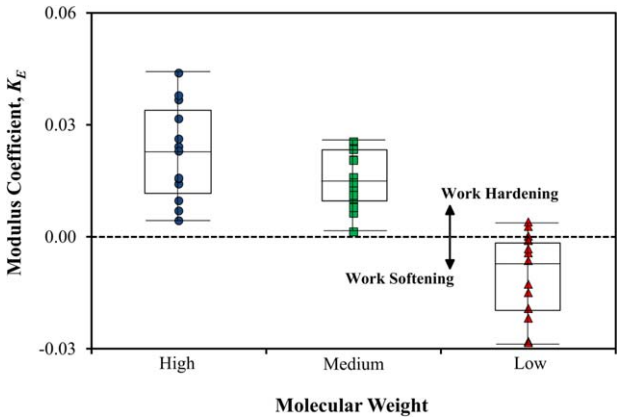

Figure 6. Modulus coefficient (i.e., the logarithmic proportionality constant of the curve fit to the time-dependent development of the elastic modulus having units of GPa per ln(cycles)) as a function of the molecular weight. The overlaid box plots represent an analysis of variance test, with each data point representing a single test sample. [Color figure can be viewed in the online issue, which is available at wileyonlinelibrary.com.]

confidence interval over 99%. The dependence on MW indicates that the development of the elastic modulus is dominated by deformations in the amorphous regions. Two competing mechanisms could be responsible for the changes in the modulus during cyclic loading. First, hysteretic heating would continue to result in a general material softening. Second, as permanent deformation continues, preferential alignment of the amorphous tie chains in the direction of loading could lead to a general material hardening. It can be seen by examining Figure 6 that, after the initial material softening, alignment of molecular chains begins to show dominance at higher MWs, whereas hysteretic heating continues to dominate at lower MWs. The variations observed between the MWs can be attributed to differences in the length of the polymer chains and tie molecules. Increasing the MW of a polymer increases the amount and length of tie molecules.[28] Longer polymer chains allow increased amorphous region movement and reorientation before becoming disentangled, providing the observed increase in strength.

Plastic Work Analysis. In addition to the modulus analysis, the detailed hysteretic behavior was examined to determine the relative contributions of elastic and plastic work. The dissipated energy (i.e., the plastic work) for a given cycle can be found by integrating the area inside one of the hysteresis loops as described by eq. (4) and shown in Figure 2. Figure 7 shows dissipated energy data for characteristic high, medium, and low displacements as a function of the number of loading cycles. Data are shown for (a) high, (b) medium, (c) and low MW POM. For clarity, only a selected number of displacements are shown in Figure 7. It can be seen that increases in the displacement lead to an increase in energy dissipated per loading cycle. This is expected because higher displacements result in increased plastic deformation.

The amount of energy dissipated displays a log-linear decrease as a function of the number of loading cycles. The energy dissipation behavior is attributed, in part, to the testing being performed at a constant displacement. As plastic deformation occurs in this type of unilateral constant displacement testing, the subsequent cycles will have a decrease in the total amount of energy input and a corresponding decrease in the plastic work. To quantify the log-linear decrease observed in Figure 7, a logarithmic curve fit was performed, and the proportionality

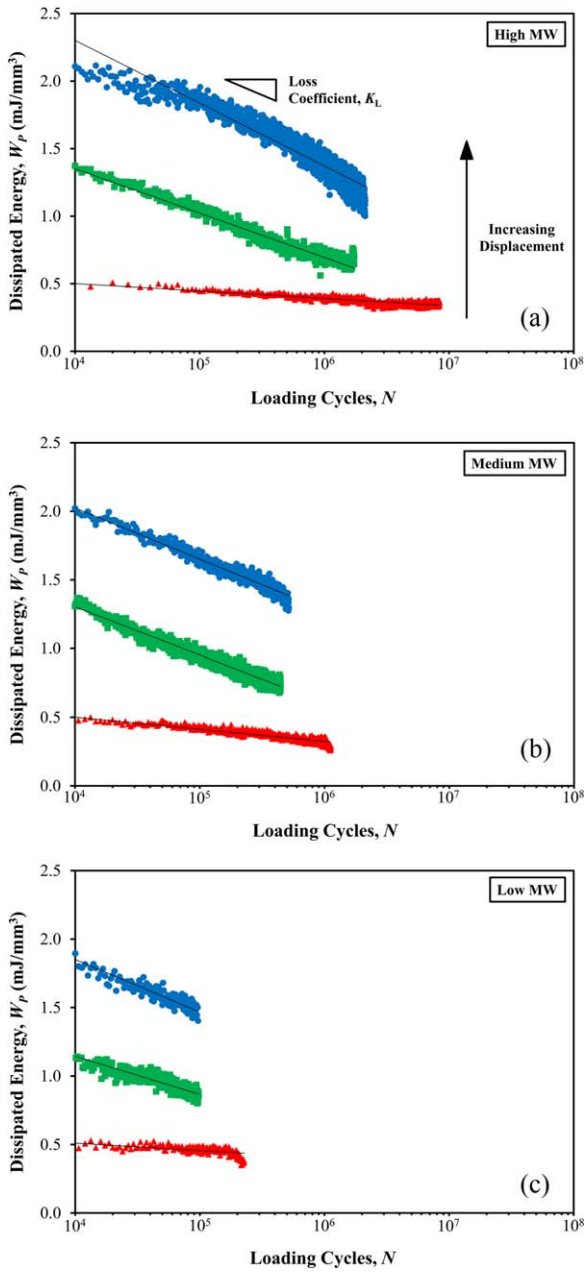

Figure 7. Characteristic data for irreversible work as a function of the number of bending fatigue cycles for (a) high, (b) medium, and (c) low molecular weight samples. Data are shown for each polymer type at maximum displacement magnitudes of (○) 6 mm, (□) 5 mm, and (Δ) 3 mm. [Color figure can be viewed in the online issue, which is available at wileyonlinelibrary.com.]

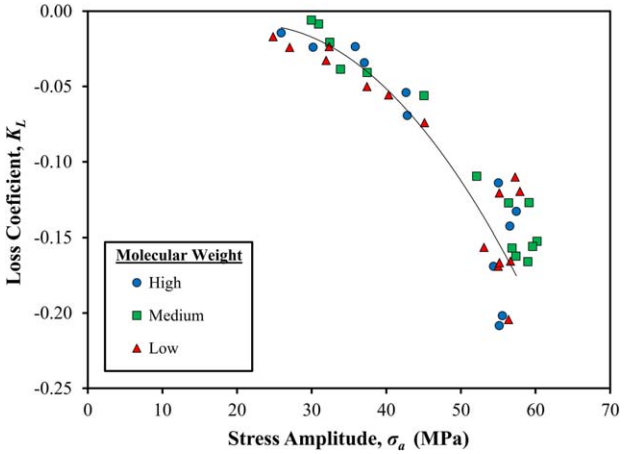

Figure 8. Loss coefficient (i.e., the proportionality constant of the logarithmic curve fit to the development of the dissipated energy, having units of mJ/mm^3 per ln(cycles)) as a function of the stress amplitude. Each data point represents a measurement of a single sample tested at a single displacement level. [Color figure can be viewed in the online issue, which is available at wileyonlinelibrary.com.]

constant will be termed the loss coefficient, K_L, having units of mJ/mm^3 per ln(cycles). Figure 8 shows the loss coefficient as a function of the measured average stress amplitude, with each data point representing the loss coefficient for a single test. As stress decreases, the plastic work per cycle remains relatively stable, and the loss coefficient approaches zero. At high stress levels, significant permanent deformation with each successive cycle results in a decreased load-bearing capacity. Accordingly, a rapid decrease in the plastic work (i.e., a highly negative loss coefficient) and total input energy is observed. This hypothesis is further supported by observing the apparent stress limit at approximately 60 MPa. Even as strain is increased, additional load-bearing capacity is inhibited.

By comparing Figure 7(a–c) and examining Figure 8 it can also be concluded that the dissipation energy is independent of MW. Accordingly, the molecular deformation mechanism is related to behavior in the crystalline region rather than in the amorphous region. This is expected because deformation and separation of the lamellae in the crystalline regions require more energy than deformation of an equivalent volume of amorphous material. Therefore, it is not surprising that the development of the dissipation energy is dominated by crystalline behavior and, thus, shows a negligible dependence on MW. Lamellar breakdown was qualitatively observed via crazing at the tension surface.

Because samples experience permanent deformation during testing, along with a corresponding change in the equilibrium relaxed position, the material property development was studied by analyzing the ratio of dissipated energy to total input energy, known as specific loss [see eq. (6)]. Figure 9 shows the specific loss as a function of the number of loading cycles. Tests are shown for selected maximum displacement magnitude of (a) high, (b) medium, and (c) low MW POM.

Several observations can be made regarding the data in Figure 9. The first is that the specific loss does not change markedly throughout a given test, indicating that the viscoelastic properties of the material are not significantly affected during a test. In other words, the phase angle, δ, remains relatively unchanged throughout testing, indicating a stable balance between stiffness and dynamic damping components. This, combined with the fact that the stiffness component, i.e., the modulus, is seen to change throughout testing (see Figures 5 and 6); points toward a corresponding alteration in the material damping components. Thus,

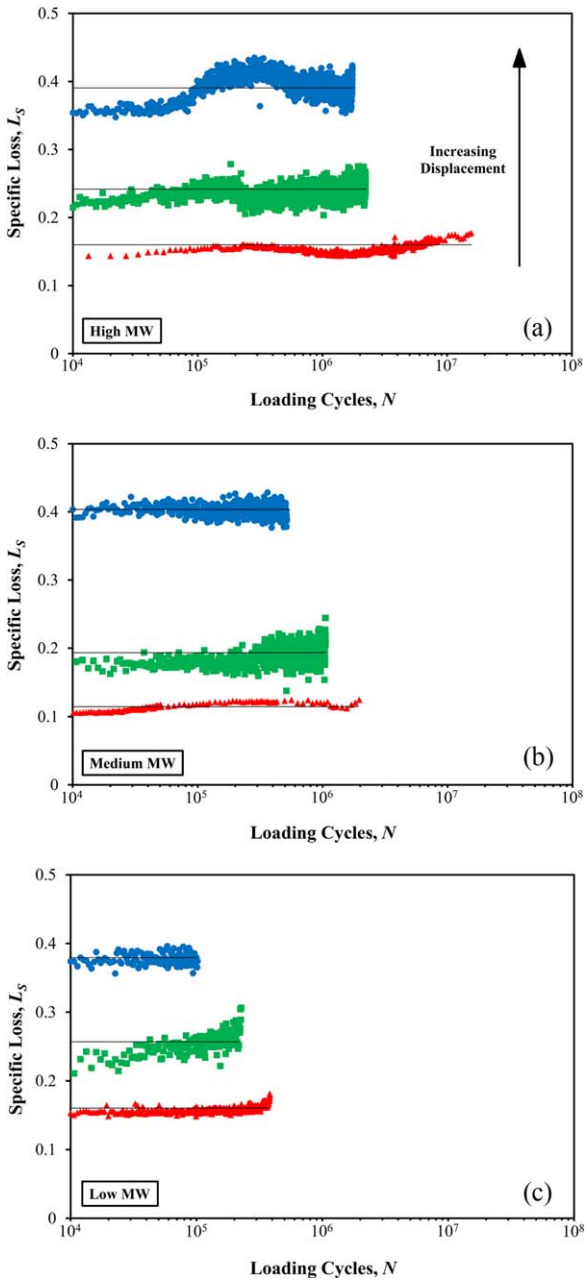

Figure 9. Characteristic data for specific loss, i.e., the ratio of the irreversible work to the total input strain energy, as a function of the number of bending fatigue cycles for (a) high, (b) medium, and (c) low molecular weight samples. Data are shown for each polymer type at maximum displacement magnitudes of (○) 6 mm, (□) 3 mm, and (Δ) 2 mm. [Color figure can be viewed in the online issue, which is available at wileyonlinelibrary.com.]

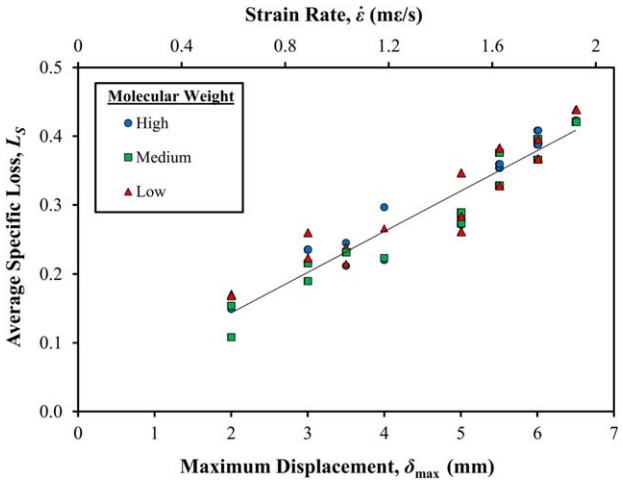

Figure 10. Average specific loss vs. maximum displacement and corresponding strain rate. Each data point represents a measurement of a single sample tested at a single displacement level. [Color figure can be viewed in the online issue, which is available at wileyonlinelibrary.com.]

although both elastic and viscous forces can change significantly, the viscoelastic behavior remains relatively constant for a given displacement or strain rate. A second observation is that specific loss increases with increasing maximum displacement. This could be attributed to two possible sources. First, the balance between elastic and viscous properties could be affected by the significantly enhanced plastic deformation at high displacements. However, because plasticity is seen to change throughout a given test (see Figure 8), whereas no corresponding change is seen in the specific loss, plastic deformation is thought to be a secondary source of the displacement dependency. The second potential source is the change in strain rate. Increasing the displacement at a constant cyclic loading frequency results in an unavoidable increase in strain rate. Because viscoelastic properties are known to be highly strain rate dependent, this is likely the primary source of the observed displacement dependency.

In order to quantify the viscoelastic properties, the average specific loss was plotted as a function of the maximum displacement as shown in Figure 10. Because the tests were performed at a constant cyclic frequency of 6.67 Hz, each maximum displacement corresponds to a unique average strain rate. Accordingly, the strain rate is shown as the secondary axis in Figure 10. Specific loss can be seen to increase linearly with increasing strain rate, showing that the phase lag, internal damping, and relative contribution of plasticity are increasing. It also should be noted that there is no substantial dependence of the viscoelastic properties on the MW. These results are in agreement with previous theoretical[20,21] and experimental[22,25] research showing that similar viscoelastic behavior is exhibited by different MW polymers with the same dispersity. This indicates that the viscoelastic behavior is dominated by the properties of the crystalline regions and that the amorphous regions have a secondary effect on viscoelasticity.

Fatigue Life Analysis. In addition to examining the development of the elastic and plastic material properties, the cyclic loading failure limits were measured in order to link fatigue behavior with the corresponding molecular deformation mechanisms. Figure 11 shows the stress amplitude vs. the cycles to failure. The fatigue life behavior of each polymer class was characterized using a stress–life curve.

$$\sigma_a = \sigma_f' \left(2N_f\right)^b \tag{7}$$

where, σ_a is the stress amplitude (equal to the one half of the maximum stress in the current, unidirectional tests), N_f is the number of cycles to failure, and σ_f' and b are the fitting parameters. The fitting constants for the stress–life curve are shown in Table II. Although ductile metals often display a proportionality constant, σ_f', approximately equal to the fracture strength of the material, this relationship is not exhibited in the current tests. Instead, proportionality constants of 9–10 GPa are observed for materials whose reported tensile strength levels are on the order of 10–100 MPa. The discrepancy is accounted for by considering the fundamental mechanistic differences between metallic and polymeric molecular deformations in fatigue and tensile conditions. In the current fatigue experiments, significant time, coupled with significant input energy, allows for molecular chain reorganization. Final failures are dominated by craze regions (i.e., the final amorphous tie chains) that link lamellae and not by the strength of the crystalline regions. This is further supported by comparing the results for the low, medium, and high MW POM in Figure 11. Despite having nearly identical crystalline morphology, the three polymer classes exhibit significantly different fatigue life behavior. The development of the mechanical properties as a function of the number of loading cycles is primarily dictated by the crystalline regions (see Figures 5, 8, and 10). However, the final failure limits for the macrostructure are defined by the length of the molecular chains that connect these crystalline regions. As mechanical damage progresses and crystalline lamella dissociate, amorphous molecular chains align in the loading direction. Eventually, the fracture limit is dictated by the critical length over which these oriented chains can maintain the mechanical integrity of the macrostructure. Because high MW polymers will result in longer tie chains, a significantly longer lifetime is observed with increasing chain

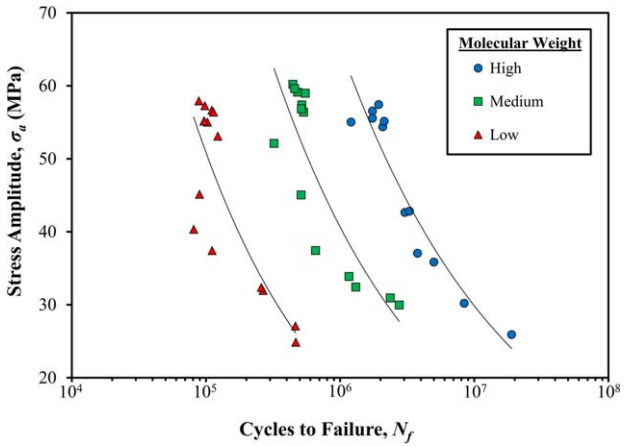

Figure 11. Average stress amplitude vs. cycles to failure for high, medium, and low molecular weight polyoxymethylene. Each data point represents a measurement of a single sample tested at a single displacement level. [Color figure can be viewed in the online issue, which is available at wileyonlinelibrary.com.]

Table II. Stress and Strain Life Curve Fitting Parameters

Polymer	σ_f' (MPa)	b	E (MPa)
High MW	9715	−0.344	701
Medium MW	8560	−0.364	748
Low MW	9952	−0.432	632

length. As such, increasing the MW in POM samples increases fatigue life while leaving zero-hour properties and viscoelastic property development patterns relatively unchanged.

Figure 12 shows the strain amplitude vs. the number of cycles to failure. Data points represent discrete tests to failure for each polymer class, and the curve fits are made according to the first term of the modified Morrow equation.[33]

$$\varepsilon_a = \frac{2\sigma_f'}{E}(2N_f)^b \tag{8}$$

where ε_a is the strain amplitude (equal to the maximum strain for the current unidirectional testing) and the additional fitting parameter E is shown in Table II. One important observation can be made by comparing the stress–life curves (Figure 11) and strain–life curves (Figure 12). By examining the low cycle regime, it can be seen that, while strain continues to increase, stress amplitude seems to reach a plateau past which additional displacement does not enhance the load-bearing capacity. The lack of a strain amplitude maximum, for the tested displacements, in conjunction with the stress amplitude limit indicates an elastic-perfectly plastic phenomenon at large displacements. The elastic-perfectly plastic behavior of the material is observed at similar strain amplitudes for each polymer class.

As seen in Table I, the principal material property distinguishing among the three tested polymers is the MW. Accordingly, the mechanical property development results can be categorized as either MW dependent or independent. The fatigue life and the logarithmic change in the modulus (i.e., the modulus coefficient) are observed to be highly dependent on MW. High MW

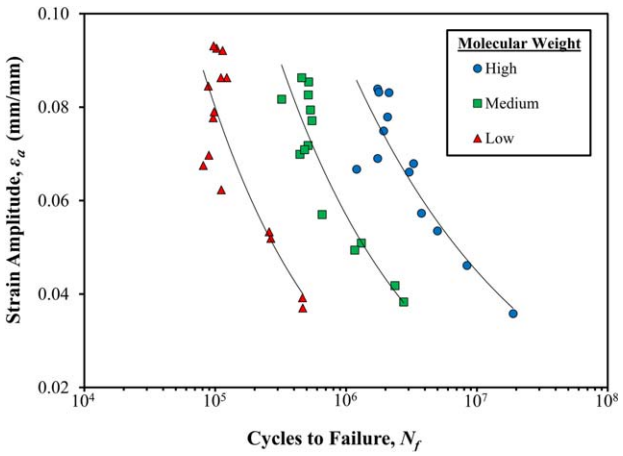

Figure 12. Average strain amplitude vs. cycles to failure for high, medium, and low molecular weight polyoxymethylene. Each data point represents a measurement of a single sample tested at a single displacement level. [Color figure can be viewed in the online issue, which is available at wileyonlinelibrary.com.]

materials yield longer fibril bridges spanning damaged areas, thereby prolonging operational life and leading to increased strain hardening. In contrast, the initial modulus decrease, dissipated energy, and viscoelastic properties are MW independent. This indicates that these phenomena are primarily dictated by deformations in the crystalline regions, the size and density of which are not significantly dependent on MW.

CONCLUSIONS

The development of the mechanical properties and the corresponding failure limits of POM under unidirectional cyclic bending was examined. Based on the current cyclic testing results, along with analytical measurements of the thermodynamic and morphological properties, the following main conclusions can be made:

1. Alterations in the MW of POM have little effect on the percentage crystallinity, melt temperature, and lamella thickness in injection-molded samples.
2. During cyclic loading, the elastic modulus experiences a rapid decrease in the early testing stages, followed by a slower rate stress hardening or softening effect. The first-stage behavior is independent of MW (indicating behavior dictated by the crystalline regions), whereas the second stage is dependent on MW (indicating behavior dictated by amorphous regions).
3. The development of plastic and viscoelastic properties is shown to be independent of MW, indicating a behavior dominated by molecular deformations in the crystalline regions.
4. The failure limits in cyclic fatigue display a strong dependence on MW. This indicates that the development of the mechanical properties is dictated by molecular deformations in the crystalline regions, whereas final fracture limits are determined by the length of the amorphous tie chains that link these crystalline regions.

ACKNOWLEDGMENTS

This research was carried out with funding and support provided by Winzeler Gear. E. I. du Pont de Nemours and Company (DuPont) generously provided the test samples, as well as execution of the differential scanning calorimetry and size exclusion chromatography testings. The authors also thank John Winzeler and Mike Cassata of Winzeler Gear, Dr. W. Dan Saunders of DuPont, and Dr. Martin Morris of Bradley University for valuable guidance and discussion.

REFERENCES

1. Wissbrun, K. F. *Polym. Eng. Sci.* **1983**, *23*, 216.
2. Postema, A. R.; Smith, P. *ACS Polym. Preprints.* **1989**, *30*, 301.
3. Chang, F. C.; Yang, M. Y. *Polym. Eng. Sci.* **1990**, *30*, 543.
4. Heckele, M.; Schomburg, W. K. *J. Micromech. Microeng.* **2004**, *14*, R1–R14.
5. Tsukamoto, N.; Maruyama, H.; Mimura, H.; Ebata, Y. *Japan Soc. Mech. Eng.* **1993**, *36*, 241.

6. Bartczak, Z.; Cohen, R. E.; Argon, A. S. *Macromolecules* **1992**, *25*, 4692.
7. Vogiatzoglou, S.; Barton, D. C.; Mohanraj, J. *Plast. Rubber Compos.* **2010**, *39*, 256.
8. Peterlin, A. *J. Mater. Sci.* **1971**, *6*, 490.
9. Halary, J. L.; Laupretre, F.; Monnerie, L. Polymer Materials: Macroscopic Properties and Molecular Interpretations; Wiley: Paris, **2011**.
10. Ferry, J. D. Viscoelastic Properties of Polymers; Wiley: New York, **1970**.
11. Shultz, J. M. Polymer Material Science; Prentice-Hall: Englewood Cliffs, NJ, **1974**.
12. Plummer, C. J. G.; Menu, P.; Cudre-Mauroux, N.; Kausch, H. H. *J. Appl. Polym. Sci.* **1995**, *55*, 489.
13. Plummer, C. J. G.; Cudre-Mauroux, N.; Kaush, H. H. *Polym. Eng. Sci.* **1994**, *34*, 318.
14. Lesser, A. J. *J. Appl. Polym. Sci.* **1995**, *38*, 869.
15. Crawford, R. J.; Benham, P. P. *Polymer* **1975**, *16*, 908.
16. Shariati, M.; Hatami, H.; Eipakchi, H. R.; Yarahmadi, H.; Torabi, H. *Polym. Plast. Tech. Eng.* **2011**, *50*, 1576.
17. Crawford, R. J.; Benham, P. P. *J. Mater. Sci.* **1974**, *9*, 18.
18. Lazzeri, A.; Marchetti, A.; Levita, G. *Fatigue Fract. Eng. Mater. Struct.* **1997**, *20*, 1207.
19. Doi, M.; Edwards, S. F. The Theory of Polymer Dynamics; Oxford University Press: Oxford, **1986**.
20. de Gennes, P. G. *J. Chem. Phys.* **1971**, *55*, 572.
21. Rubinstein, M. *Phys. Rev. Lett.* **1987**, *59*, 1946.
22. Ruymbeke, E.; Keunings, R.; Stephenne, V.; Hagenaars, A.; Bailly, C. *Macromolecules* **2002**, *35*, 2689.
23. Graessley, W. W. *J. Polym. Sci. Polym. Phys. Ed.* **1980**, *18*, 27.
24. Montfort, J. P.; Marin, G.; Monge, PH. *J. Am. Chem. Soc.* **1986**, *19*, 1979.
25. Tsenoglou, C. *Macromolecules* **1991**, *24*, 1762.
26. Connolly, R.; Gauvin, R.; Chalifoux, J. P. *Polym. Eng. Sci.* **1985**, *25*, 548.
27. Bretz, P. E.; Hertzberg, R. W.; Manson, J. A. *J. Appl. Polym. Sci.* **1982**, *27*, 1707.
28. Huang, Y. L.; Brown, N. *J. Polym. Sci.* **1991**, *29*, 129.
29. Huang, Y. L.; Brown, N. *J. Polym. Sci.* **1990**, *28*, 2007.
30. Huang, Y. L.; Brown, N. *J. Mater. Sci.* **1988**, *23*, 3648.
31. Bensason, S.; Minick, J.; Moet, A.; Chum, S.; Hiltner, A.; Baer, E. *J. Polym. Sci.* **1996**, *34*, 1301.
32. Palza, H.; Lóépex-Majada, J. M.; Quijada, R.; Benavente, R.; Pérez, E.; Cerrada, M. L. *Macromol. Chem. Phys.* **2005**, *206*, 1221.
33. Morrow, J. D. ASTM STP378, **1964**.